Ultrafast Dynamics of Electron Thermalization in Gold

Chunlei Guo,* George Rodriguez, and Antoinette J. Taylor
Los Alamos National Laboratory, Los Alamos, New Mexico 87545
(Received 21 April 2000)

Time-resolved surface second-harmonic generation (SHG) is used to probe electron relaxation processes in gold following intense laser excitation at 1.55 eV. For the first time, an electron temperature (T_e) dependent enhancement in the SHG signal is clearly observed at T_e above 0.7 eV, which is shown to relate to the thermalization of nonequilibrium hot electrons. Therefore, the relaxation dynamics of the transient nonequilibrium electrons in the high T_e regime is directly resolved by monitoring the time evolution of the SHG signal.

DOI: 10.1103/PhysRevLett.86.1638 PACS numbers: 78.47.+p, 72.15.Lh, 78.40.Kc

Our understanding of femtosecond laser interactions with metals is largely based on the so-called two-temperature model (TTM) [1]. Since the heat capacity of the electrons is much smaller than that of the lattice, an ultrashort laser pulse, with a duration less than the excited electron energy-loss lifetime, can heat electrons in a metal to a very high temperature while leaving the lattice relatively cool. In most cases, thermalization of the hot electrons can be assumed to occur instantaneously due to the short electron-electron interaction time. Therefore, the overall picture of a nonequilibrium system in metals is normally described as constituting two subequilibrium systems, the hot electrons and a cold lattice [1]. This transient two-temperature system will tend to reach equilibrium within a few picoseconds through electron-phonon interactions as well as electron transport out of the excited region. The dynamics of the electron-phonon interaction based on TTM is relatively well understood through extensive studies during the past two decades [2–4]. The early stages of the electron thermalization process have also been studied but under more restricted conditions, where the assumption of instantaneous thermalization of the hot electron subsystem immediately after laser excitation has been shown to be invalid [5,6]. However, study in ultrafast dynamics of electron thermalization has been limited [e.g., in the relatively low electron temperature (T_e) regime] by experimental difficulties (e.g., space charge effects in the photoemission measurements in the high T_e regime) with conclusions normally drawn from very subtle deviations between experimental data and model predictions [5,6]. Therefore, the development of new techniques to reveal the character of this noninstantaneous thermalization within the electron subsystem is desirable. It is especially important to extend these studies to the high T_e regime to gain further information on a variety of high T_e phenomena that relate to structural phase transitions, laser-induced desorption, micromachining, ablation, and photochemistry.

In this paper, we describe a pump-probe optical measurement that reveals the details of hot electron thermalization dynamics by monitoring the time evolution of both the fundamental probe reflectivity at 1.55 eV and the second harmonic generation (SHG) at 3.1 eV from a gold (Au) surface. A T_e dependent enhancement of surface SHG is observed, for the first time in the high T_e regime (T_e over 1 eV with the input energy just below melting threshold in Au; this temperature is more than 30 times higher than those in previous measurements [5,6]), as a result of thermalization of the hot electron subsystem induced by intense pump laser excitation.

The experimental setup follows those described in Refs. [7,8]. Briefly, we perform cross-polarized (p polarization for probe) pump-probe measurements with an amplified Ti:sapphire laser system delivering 110 fs pulses with a central wavelength of 800 nm. The pump beam is weakly focused near normal incidence onto the sample, while the probe beam, incident at 52°, is focused to an area ~10 times smaller than that of the pump beam. Surface SHG is generated by the weak probe beam that does not cause any modification of the sample. The collinearly propagated reflected fundamental and SHG beams are separated by a dichroic beam splitter and simultaneously monitored after bandpass filtering. As will be described later, we are particularly interested in deviations of the surface SHG signal due to the nonequilibrium electron distribution. Therefore, the SHG data are not normalized to the fundamental energy by assuming a quadratic intensity dependence. Rather, an intensity window circuit is used to restrict the data collection to within a fluctuation range of 5% for a certain incident pulse energy. The Au sample used in these experiments is a polycrystalline, optical film prepared by high vacuum deposition.

Multishot pump-probe measurements are used to eliminate any artificial response in the first few shots due to the possible surface contamination, and the measurements are repeated for different locations on the Au sample. By increasing the pump pulse intensity to right below the melting threshold for Au, the hot electron dynamics can be resolved by studying both the fundamental and SHG signals for T_e up to ~1.1 eV. T_e is estimated by assuming that all the absorbed energy at 800 nm is stored in an electron gas with an optical skin depth of 20 nm [9,10]. It is reasonable to assign this peak temperature to that of the surface probed by SHG. The bulk temperature

 0031-9007/01/86(8)/1638(4)$15.00

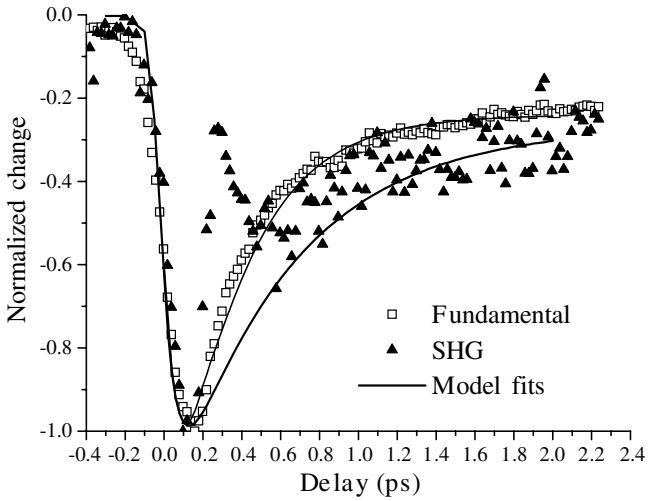

FIG. 1. Time-resolved fundamental and surface SHG signals at a pump-induced T_e of 1.03 eV. The solid lines are the model fits to the fundamental signal and the SHG signal by considering only the T_e dependence of the Fresnel factors.

sampled by the fundamental light over the skin depth is smaller, and this leads to a different electron-phonon coupling time between the fundamental and SHG signals in Fig. 1. (Note that the temperature is an ill-defined quantity for a nonequlibrium system. When a temperature is quoted, it always refers to the final temperature when equilibrium is reached by assuming no energy is lost during the thermalization process.) The time-resolved fundamental and surface SHG signals, both from the probe pulse, are plotted in Fig. 1 for Au exposed to a pump intensity of 1.3×10^{12} W/cm^2. Both signals initially decrease after pump excitation; they each reach minimum values, and then begin to recover. The fundamental reflectivity signal recovers monotonically to a relatively constant value within a few picoseconds. The SHG signal, however, after reaching the minimum, rises to a local maximum and then drops down again, showing a temporal local peak structure at a pump-probe time delay of approximately 260 fs. In Fig. 2, we plot the time-resolved SHG signals for three T_e. For $T_e = 0.58$ eV, the SHG signal recovers monotonically and no local enhancement is observed. At T_e above 0.7 eV, a local maximum appears in the SHG signal and this peak structure becomes more pronounced with increasing T_e. The temporal position of this local maximum in the SHG signal also shifts to shorter delay times as T_e increases, e.g., the peak of the SHG signal is at 310 fs for $T_e = 0.87$ eV, but shifts to 260 fs for $T_e = 1.03$ eV.

Since the onset of the major interband transitions in Au (2.45 eV) significantly exceeds the fundamental laser photon energy (1.55 eV), the dominant effect of the pump pulse results in an ultrafast heating [8,11]. The decrease in the fundamental and SHG probes after laser excitation is due to this heating, consistent with previous observations [8,12]. The ensuing relaxation of probe signals on a picosecond time scale is due to the electron-phonon coupling as described above by TTM. However, an explanation of the reproducible local peak of the SHG signal ~300 fs after pump excitation requires a mechanism not incorporated in TTM. Since this local peak persists in the SHG signal but is absent in the fundamental signal, we first need to consider the possibility of accidental coupling to surface states. However, the experiment is performed with a polycrystalline sample in air and, therefore, coupling to surface states is very unlikely since surface states are normally associated with well-defined ordered surfaces. We can also eliminate one or two photon resonant effects since any resonance occurs instantaneously following the laser radiation, inconsistent with the experimentally observed time delay of ~300 fs for the enhancement in SHG. Furthermore, the systematic observation of this surface SHG enhancement (verified on different sample locations) eliminates any experimental artifacts and requires that the enhancement in the SHG signal be attributed to an intrinsic physical mechanism.

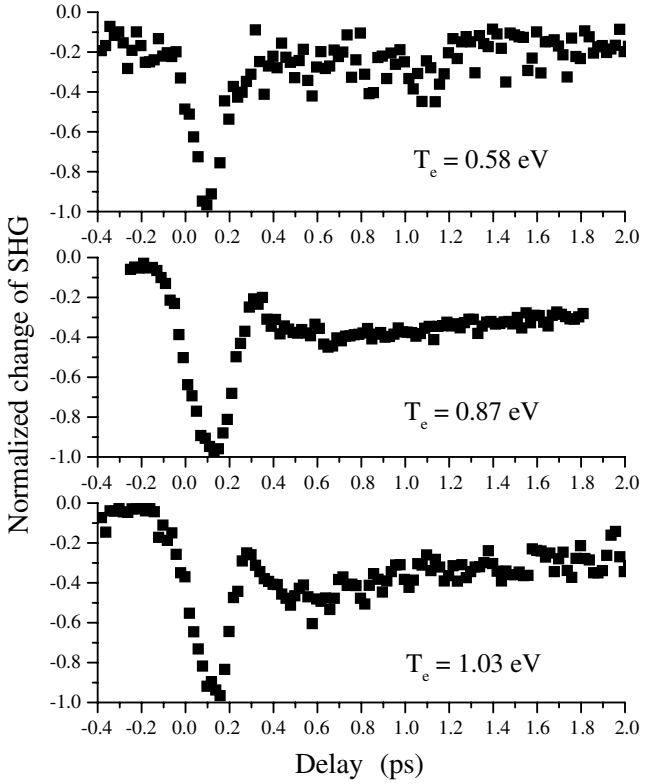

FIG. 2. Time-resolved SHG signal at three different T_e.

In order to understand the temporal structure of the SHG signal following the pump excitation, we evaluate the magnitude of the surface SHG signal by using a phenomenological model from Ref. [13]. For the p-polarized incident probe pulse in our experiments, it has been verified that the term with χ_{zzz} dominates the SHG process for polycrystalline metals [14,15]. Therefore, the SHG amplitude can be expressed as

$$E(2\omega, T_e) \propto F(2\omega, T_e)\chi^{(2)}_{zzz}(T_e) f(\omega, T_e)\,|E_p(\omega)|^2 = T_p(T_e)\epsilon(2\omega, T_e)F_s(T_e)\chi^{(2)}_{zzz}(T_e) f_s^2(T_e)\epsilon^2(\omega, T_e)t_p^2(T_e)\,|E_p(\omega)|^2. \quad (1)$$

The SHG signal depends on linear Fresnel factors at both the fundamental and second harmonic frequencies, $f(\omega, T_e)$ and $F(2\omega, T_e)$, and surface second-order nonlinear susceptibility, $\chi^{(2)}_{zzz}(T_e)$. The abbreviations $f_s(T_e) = \sin\theta/[\epsilon(\omega, T_e)]^{1/2}$, $f_c(T_e) = (1 - [f_s(T_e)]^2)^{1/2}$, and $t_p(T_e) = 2\cos\theta/[(\epsilon(\omega, T_e))^{1/2}\cos\theta + f_c(T_e)]$. The angle, θ, denotes the angle of incidence. Equivalent expressions for $F_s(T_e)$, $F_c(T_e)$, and $T_p(T_e)$ with $\epsilon(2\omega, T_e)$ are used. Note that all the quantities in Eq. (1) are T_e dependent. Therefore, the T_e dependence of both the Fresnel factors and nonlinear susceptibility determines the temporal dependence of SHG.

To understand the time evolution of SHG, we first determine the time dependence of T_e by solving the coupled differential equations using TTM [16]. In order to disentangle the temperature effects on SHG from different contributing elements, the temperature dependence of the linear Fresnel factors and the nonlinear second-order nonlinear susceptibility are considered separately. We assume that the nonlinear susceptibility is T_e independent and fit the change of SHG only with T_e dependent Fresnel factors. We follow Refs. [12,14,17] to obtain the temperature dependence of dielectric constant at both the fundamental and second-harmonic frequencies. The dynamics of the fundamental reflectivity and the main feature in the SHG data can be reproduced using the same set of deduced parameters (Fig. 1). However, the local peak enhancement in the SHG signal at 260 fs is not reproduced, as seen in Fig. 1. The modeled change of SHG will always be a smooth function as long as the nonlinear susceptibility, $\chi^{(2)}_{zzz}$, is assumed to be T_e independent, making it impossible to fit the enhanced structure observed in the SHG signal at 260 fs following the pump excitation. Therefore, the discrepancy between the SHG data and the model fit has to come from the dynamic T_e dependence of the nonlinear susceptibility, the only nonlinear parameter in the SHG expression.

By subtracting the experimental SHG data from the model fit obtained by considering only the Fresnel factors (both in Fig. 1), we obtain the dynamic change in the SHG signal purely due to the T_e dependent nonlinear susceptibility (see Fig. 3). This change of the SHG signal (y axis of Fig. 3) is labeled as $\triangle\chi^{(2)}$ to facilitate further discussion. Figure 3 shows that $\triangle\chi^{(2)}$ first increases to a maximum value ~260 fs after the pump laser excitation and then relaxes on a picosecond time scale. The time delay necessary for $\triangle\chi^{(2)}$ to reach a maximum value indicates that the nonlinear susceptibility does not instantaneously follow the laser-induced T_e change. To understand this, the physical origin of $\chi^{(2)}$ must be considered. The generation of second-harmonic light involves an electron at initial energy level E absorbing two photons at an optical frequency ω and then relaxing back to the initial state by emitting a photon at 2ω. Therefore, the probability for this SHG process will be proportional to an electron distribution function involving initial, intermedium, and final states, $f(E)[1 - f(E + \hbar\omega)][1 - f(E + 2\hbar\omega)][1 - f(E)]$ and the corresponding joint density of states (JDOS) for optical transitions at each energy. The effective nonlinear susceptibility incorporating this distribution and JDOS function will be [18]

$$|\chi^{(2)}_{\text{eff}}|^2 = |\chi^{(2)}|^2 \int_0^\infty f(E)[1 - f(E + \hbar\omega)] \times [1 - f(E + 2\hbar\omega)][1 - f(E)] \times \text{JDOS}(E)\, dE\,, \quad (2)$$

where $\chi^{(2)}$ is the nonlinear susceptibility in the single-electron picture [19] and the electron distribution function $f(E)$ takes into account the T_e dependence of $\chi^{(2)}_{\text{eff}}$. Note that the distribution function, $f(E)$, is not necessarily a Fermi-Dirac distribution. In fact, the initial electron distribution immediately after the pump excitation is a nonequilibrium distribution that involves the excitation of a certain number of electrons distributed within the energy range of the laser photon energy from below the Fermi level to above the Fermi level [6], as shown in inset (a) of Fig. 4. These nonequilibrium electrons will thermalize to a Fermi-Dirac distribution through electron-electron scattering [inset (b) of Fig. 4]. The T_e dependent nonlinear susceptibility $\chi^{(2)}_{\text{eff}}$ can be evaluated according to Eq. (2) for electrons in both a nonequilibrium distribution and a Fermi-Dirac distribution in Au [20], and the results are plotted in Fig. 4. Notice that $\chi^{(2)}_{\text{eff}}$ increases with T_e for both equilibrium and nonequilibrium distributions, and this fact has been confirmed by observations on the enhancement of SHG with single pulse measurements at sufficiently high laser intensities [18]. Further, the difference in the values of $\chi^{(2)}_{\text{eff}}$ between equilibrium and

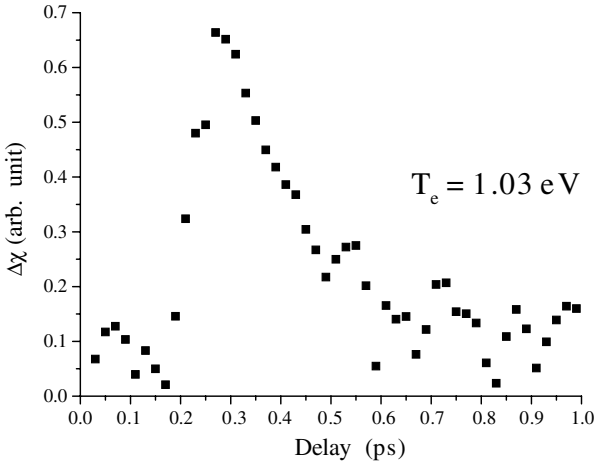

FIG. 3. The change of nonlinear susceptibility $\triangle\chi^{(2)}$ versus pump-probe time delay, obtained by subtracting the SHG model fit from the experimental SHG data at $T_e = 1.03$ eV.

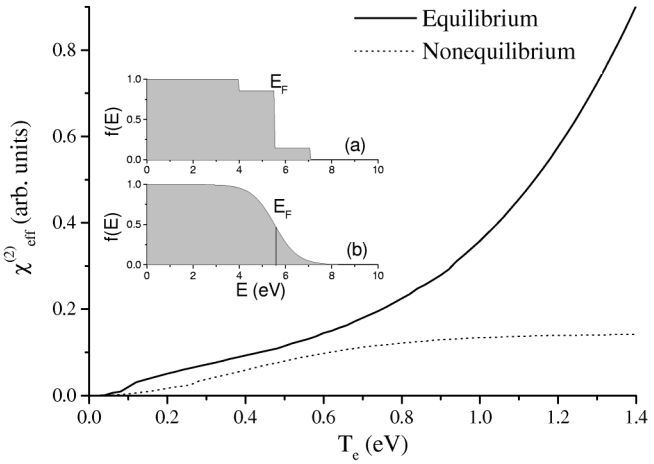

FIG. 4. Nonlinear susceptibility $\chi^{(2)}_{\text{eff}}$ versus T_e for both equilibrium and nonequilibrium distributions in Au. Inset (a) nonequilibrium electron distribution right after laser excitation; (b) hot electron distribution in thermal equilibrium.

nonequilibrium distributions is relatively small for T_e below 0.7 eV, but increases with T_e above 0.7 eV. Qualitatively similar features for $\chi^{(2)}_{\text{eff}}$ are also obtained without incorporating JDOS for Au. However, the difference of $\chi^{(2)}_{\text{eff}}$ between equilibrium and nonequilibrium distributions at high T_e is larger when considering JDOS in Au. Furthermore, this difference of $\chi^{(2)}_{\text{eff}}$ also varies when the distance between the localized d band and the Fermi level is artificially adjusted in JDOS. These simulations indicate that the d-band electrons play a role in SHG, especially when the Fermi surface is considerably smeared at high T_e to provide empty states for d-band electron transitions.

The subtle dependence of $\chi^{(2)}_{\text{eff}}$ on both T_e and the thermalization process in Fig. 4 is, in fact, directly exhibited in our experimental data. First, since the value of $\chi^{(2)}_{\text{eff}}$ is much higher for an equilibrium electron distribution than for a nonequilibrium distribution for T_e above 0.7 eV, the initial increase in $\triangle\chi^{(2)}$ at $T_e = 1.03$ eV (Fig. 3) comes from the thermalization of hot electrons from the nonequilibrium distribution relaxing to equilibrium states. This also explains why the local enhancement in the SHG signal is only observed experimentally with T_e above 0.7 eV. Subsequent electron-phonon coupling will reduce T_e and decrease $\triangle\chi^{(2)}$. Therefore, the change of the SHG signal due to the T_e dependence of $\triangle\chi^{(2)}$ directly exhibits the dynamic process of electron-electron thermalization and subsequent electron-phonon coupling. Second, the difference between $\chi^{(2)}_{\text{eff}}$ for an equilibrium electron distribution and a nonequilibrium distribution increases with T_e above 0.7 eV, clearly seen in the SHG data for three different T_e in Fig. 2: almost no local enhancement in SHG for $T_e = 0.58$ eV is observed; while the enhancement in SHG due to the electron thermalization becomes more pronounced as T_e increases (indicated by the data at $T_e = 0.87$ and 1.03 eV).

The electron thermalization time (indicated by the local peak in the SHG signals) also becomes shorter at higher T_e (260 fs at 1.03 eV; 310 fs at 0.87 eV in Au), consistent with previous observations [5]. The much shorter thermalization time we observed ($\sim$300 fs) in the high T_e regime compared to previous observations in the low temperature regime ($\sim$500 fs) is again consistent with thermalization occurring faster at higher T_e, where a larger number of electrons are involved in scattering and thermalization [5,6].

In summary, we measure the time-resolved SHG signal from Au surface following ultrafast laser excitation at 1.55 eV. For the first time, a T_e dependent enhancement in SHG is observed $\sim$300 fs after the laser excitation. This enhancement is shown to directly reflect the thermalization of hot electrons from nonequilibrium to equilibrium states. Therefore, the relaxation dynamics of hot electrons is resolved by monitoring the time evolution of the SHG signal. The resolved dynamics of highly energetic electrons in this temperature regime will fundamentally improve our understanding of electronic effects in high temperature phenomena in metals such as laser-induced structural phase transitions and chemical reactions.

We acknowledge J. Xie for communicating computational results on the electronic structure of Au. This research is performed under the auspices of the U.S. Department of Energy.

*Author to whom correspondence should be addressed. Electronic address: cguo@lanl.gov

[1] M. I. Kaganov *et al.,* Sov. Phys. JETP **4**, 173 (1957).
[2] G. L. Eesley, Phys. Rev. Lett. **51**, 2140 (1983).
[3] J. G. Fujimoto *et al.,* Phys. Rev. Lett. **53**, 1837 (1984).
[4] H. E. Elsayed-Ali *et al.,* Phys. Rev. Lett. **58**, 1212 (1987).
[5] W. S. Fann *et al.,* Phys. Rev. Lett. **68**, 2834 (1992); W. S. Fann *et al.,* Phys. Rev. B **46**, 13 592 (1992).
[6] C.-K. Sun *et al.,* Phys. Rev. B **48**, 12 365 (1993); C.-K. Sun *et al.,* Phys. Rev. B **50**, 15 337 (1994).
[7] C. Guo *et al.,* Phys. Rev. Lett. **84**, 4493 (2000).
[8] C. Guo and A. J. Taylor, Phys. Rev. B **62**, 11 921 (2000).
[9] J. R. Reitz *et al., Foundations of Electromagnetic Theory* (Addison-Welsley, Reading, MA, 1980).
[10] K. L. Moore and T. D. Donnelly, Opt. Lett. **24**, 990 (1999).
[11] C. Guo and A. J. Taylor, Phys. Rev. B **62**, 5382 (2000).
[12] J. Hohlfeld *et al.,* Appl. Phys. A **60**, 137 (1995).
[13] J. E. Sipe *et al.,* Phy. Rev. B **35**, 1129 (1987).
[14] J. Hohlfeld *et al.,* Appl. Phys. B **63**, 541 (1996).
[15] G. Petrocelli *et al.,* Appl. Phys. A **56**, 263 (1993).
[16] S. I. Anismov *et al.,* Sov. Phys. JETP **39**, 375 (1975).
[17] S. S. Jah and C. S. Warke, Phys. Rev. **153**, 751 (1967).
[18] N. A. Papadogiannis and S. D. Moustaizis, Opt. Commun. **137**, 174 (1997).
[19] J. Ducuing and C. Flytzanis, in *Optical Properties of Solids,* edited by F. Abelés (North-Holland, Amsterdam, 1972), Chap. 12.
[20] Density of states in Au is provided by J. Xie (private communication).